IEEE Access
Multidisciplinary | Rapid Review | Open Access Journal

Received October 5, 2018, accepted October 31, 2018, date of publication November 5, 2018, date of current version December 3, 2018.

*Digital Object Identifier 10.1109/ACCESS.2018.2879521*

# Semi-Supervised Cerebrovascular Segmentation by Hierarchical Convolutional Neural Network

**FENGJUN ZHAO[1], YIBING CHEN[1], FEI CHEN[2], XUELEI HE[1], XIN CAO[1], YUQING HOU[1], HUANGJIAN YI[1], XIAOWEI HE[1], AND JIMIN LIANG[2], (Member, IEEE)**

[1]School of Information Sciences and Technology, Northwest University, Xi'an 710069, China
[2]School of Life Science and Technology, Xidian University, Xi'an 710071, China

Corresponding authors: Huangjian Yi (yhj2014@nwu.edu.cn), Xiaowei He (hexw@nwu.edu.cn), and Jimin Liang (jimleung@mail.xidian.edu.cn)

This work was supported in part by the National Natural Science Foundation of China under Grant 61601363, Grant 11571012, Grant 81530058, and Grant 61701403, in part by the National Key Research and Development Program of China under Grant 2016YFC1300300, in part by the Natural Science Research Plan Program in Shaanxi Province of China under Grant 2017JQ6017, Grant 2017JQ6006, Grant 2015JM6322, and Grant 2015JZ019, and in part by the Special Research Project of Shaanxi Provincial Department of Education under Grant 16JF026, Grant 17JF027, Grant 18JK0778, and Grant 18JK0767, and in part by the China Postdoctoral Science Foundation under Grant 2016M602851, and 2018M643719.

**ABSTRACT** Due to the tortuosity and the complexity of cerebral vasculature and the similar intensity distribution with the background, it remains challenging to accurately segment cerebral vessels from magnetic resonance angiography (MRA). The previous rule-based methods have limitations when applied to accurate clinical diagnosis, such as the under-segmentation on complex vessels, the dependence on domain knowledge, and the lack of quantification estimation. In this paper, we proposed a semi-supervised cerebrovascular segmentation method with a hierarchical convolutional neural network (H-CNN) that transfers the exquisite model/feature design in rule-based methods to solve the mapping from MRA images to cerebral vessels. First, we generated the tube-level labels of cerebral vessels with centerlines and estimated radii. Second, we constructed and trained an H-CNN with the MRA images and corresponding tube-level labels. Third, the stopping criterion of the proposed H-CNN was determined by the comprehensive index (CI) that was defined based on partially annotated voxel-level ground truth. The comparison of our H-CNN with the vesselness, bi-Gaussian, optimally oriented flux, vessel enhancing diffusion, hybrid diffusion with continuous switch, Mimics software, convolutional neutral network$_{2D}$ $(CNN)_{2D}$, and $CNN_{3D,}$ were conducted on six testing images. The mean sensitivity, accuracy, and the CI of our H-CNN are 94.69%, 97.85%, and 2.99%, respectively, outperforming the other methods. The curved planar reformation also visualized the performance of H-CNN for cerebrovascular segmentation. Given only the tube-level labels, the proposed H-CNN method accomplished the voxel-level vessel segmentation via the hierarchical update of CNN. The H-CNN can potentially to be applied for the accurate diagnosis of cerebrovascular diseases and other medical image segmentation with only partially correct labels.

**INDEX TERMS** Magnetic resonance angiography, cerebral blood vessel, centerline, segmentation, convolutional neural network.

## I. INTRODUCTION

Cerebrovascular diseases, such as stroke, aneurysm, and arteriovenous malformation, have been one of the most serious diseases threatening human health, due to the high morbidity and mortality [1]–[3]. Medical imaging of cerebral vasculature provides an efficient tool to diagnose these diseases. Compared with X-ray angiography and computed tomography angiography (CTA), magnetic resonance angiography (MRA) allows a non-invasive three dimensional (3D) imaging of cerebral vessels, thus enables its application in diagnosis and surgical planning of cerebral diseases [4]. Nevertheless, accurate analysis of cerebral vessels remains challenging, due to the similar intensity distribution between vessels and the background, as well as the tortuosity and complexity of cerebral vasculature [5]. To solve this problem, numerous researches have been dedicated to the automatic or semi-automatic cerebrovascular segmentation, which can be classified into four main categories: vessel enhancement, statistical approaches, deformable models and hybrid methods.

### A. VESSEL ENHANCEMENT

Cerebral vessels generally manifest as thin, elongating, and bright structures in MRA images. Frangi *et al.* [6] and Sato *et al.* [7] enhanced vessel structures using the multi-scale vesselness filtering. The filter analyzes the Hessian matrix of an image with adaptive orientation selection, and has the ability to distinguish vessels from planar or blob-like structures [8], [9]. Subsequently, vessel enhancing diffusion (VED) was used to enhance the cerebral vasculature, which combined a smooth vessel filter with a nonlinear anisotropic diffusion scheme [10]. VED outperforms the conventional multi-scale vessel filtering on time-of-flight MRA images. Nevertheless, these vesselness filtering-based methods fail to detect small or malformed vessels. Therefore, Forkert *et al.* [11] proposed to combine the vesselness filtering and a fuzzy logic-based method with analytically designed rules, to improve the segmentation of small and malformed vessels. There are lots of other enhancement techniques, including line-shaped profiling [12], optimally oriented flux [13], ranking orientations responses path operator [14], regularize Perona-Malik approach [15], hybrid diffusion with continuous switch [16], and white top hat algorithm [17]. As a pre-processing procedure, these vessel enhancement algorithms improved the distinguishability between cerebral vessels and the background, so as to facilitate accurate cerebrovascular segmentation [18].

### B. STATISTICAL APPROACHES

The intensity histogram of brain MRA images generally consists of three regions: low intensity region (air, cerebrospinal fluid and bones), medium intensity region (white matter and gray matter), and high intensity region (cerebral vessels and subcutaneous fat) [19]. The task of statistical approach is to fit a suitable finite mixture model (FMM) to the intensity histogram. Wilson and Noble fitted a uniform distribution function to the distribution of vessel voxels and fitted two Gaussian distribution functions to the distribution of other tissues [20]. Further, Hassouna *et al.* [21] used a Gaussian distribution function to model cerebral vessels and used two Gaussian distribution functions and a Raleigh distribution function to model the other tissues. Thereby, the problem of cerebrovascular segmentation reduces to estimating the parameters of FMM. Expectation maximization (EM) algorithm was preliminarily used for parameter estimation [22]. However, it becomes time-consuming when there are too many distributions in the model. The particle swarm optimization (PSO) algorithm was adopted to parallelize the parameter estimation, which improved the efficiency of FMM fitting [19], [23]. Hao *et al.* [24] accelerated the segmentation speed by using a localized observation model rather than the global observation. The other FMMs for cerebrovascular segmentation include the Maxwell-uniform or Maxwell-Gaussian-uniform mixture model [25] and the linear combination of discrete Gaussians [26], [27]. The vascular signal loss often occur in statistical approaches due to the voxel-wise classification. A Markov random field (MRF) as the post-processing procedure can restore the lost signal by taking the regional term into account [19], [21], [23].

### C. DEFORMABLE MODELS

Deformable models attempted to approximate the boundary of vessels based on various forces that drive the curves in images [28]. The most popular deformable models are the level set methods and snakes. Developed by Chan and Vese, the level set method converts the minimal partition problem into the implicit energy minimization [29]. Manniesing *et al.* [30] used a level set-based method to find vessel boundaries from CTA images. The level set function is attracted to the vessel boundaries by different intensity distributions between vessels and background. Moreover, the geodesic active contour implemented by level set techniques was also applied to vessel segmentation from MRA images [31]. Depending on explicit evolutional formulations, snakes evolve in order to optimize a surface energy depending on image gradients and surface smoothness. Xu and Prince segmented the blood vessels using a gradient vector flow field as the additional force to drive snakes into object contours [32]. Cheng *et al.* [33] proposed an improved snake model, i.e. the constrained B-snake, and applied it to the segmentation of blood vessels from CTA with low contrast. Both the level set methods and snakes can be implemented automatically or interactively for vessel segmentation. However, they are sensitive to initializations, leading to the under-segmentation for thin and elongated cerebral vessels [34].

### D. HYBRID METHODS

The hybrid methods mainly manifest as the combination of the multi-scale vesselness filtering and other segmentation methods (deformable models or statistical approaches). For example, Descoteaux *et al.* [35] and Forkert *et al.*[36] applied the vesselness filtering to find putative centerlines and directions of tubular structures, followed by the recovery of vessel boundaries with deformable models. After vesselness filtering, Lu *et al.* [37] fitted three probabilistic distributions, two exponential distributions and one Gaussian distribution, with a FMM to the histogram curve. As a posterior probability estimation, MRF was often employed to improve the accuracy of pixel-wise classification. Xiao *et al.*[38] reconstructed the vessel image by the fusion of the traditional Bayesian statistical approach and vesselness filtering using Dempster-Shafer evidence theory. Moreover, Gao *et al.* [39] employed the statistical approach, and modeled MRA images as Gaussian distribution (cerebral vessels) and combination of a Rayleigh distribution and several Gaussian distributions (background), respectively. The result of statistical approach was used to guide the curve evolution of level set, which improves the accuracy of cerebrovascular segmentation.

Even though these methods are commonly used for cerebrovascular segmentation from MRA images, there are some limitations that preclude their accurate clinical application. (1) These methods are essentially rule-based approaches that

distinguish vessels from background by handcrafted features, such as intensity, gradient, statistics, morphology and context. In other words, both models and features of these methods require exquisite design, which heavily depend on users' domain knowledge. (2) Due to the complexity of cerebral vasculature and the similar intensity distribution with surrounding tissues, the obtained vessels are often fractured and suffer from under-segmentation, though some correction techniques for broken vessels have been devised [40], [41]. (3) Manual annotation of ground truth vessels turns out to be laborious and has considerable intra- or inter-observer errors especially on thin vessels. Therefore, most segmentation methods are just qualitatively evaluated by visual inspection. (4) Only a few quantitative evaluations have been conducted with the ground truth. However, the evaluation indices are either based on segmented cerebral blood vessels (such as Dice coefficient and Hausdorff distance) or corresponding vessel centerlines (such as the number of centerline points). An overall quantitative estimation for different segmentation methods is still absent.

Supervised methods, such as neural networks [42], support vector machines [43], random forests [44], and oblique random forests [45], treat the task of segmentation as the problem of voxel classification, which perform well for the vessel delineation in retina and rat visual cortex. However, these methods are seldom used for cerebrovascular segmentation because of the difficulty in annotating the ground truth. Meijs *et al.* [46] proposed to segment the full cerebral vasculature from computed tomography images with random forests. To evaluate the method, five sub-volumes representing different regions of the cerebral vessels were annotated by medical assistants. Moreover, with 2D annotated patches in the axial, coronal, and sagittal directions as input, Phellan *et al.*[47] trained a 2D deep convolutional neutral network (CNN) for vascular segmentation in TOF MRA images. Nevertheless, these supervised methods also require either the handcrafted features, or the labor-intensive manual annotation of all the ground truth vessels..

In this paper, we proposed a semi-supervised cerebrovascular segmentation method with a hierarchical convolutional neural network (H-CNN). Firstly, we generated the tube-level labels of cerebral vessels with centerlines and estimated radii. Secondly, we constructed and trained the H-CNN with the MRA images and corresponding tube-level labels. The stopping criterion of the proposed H-CNN was determined by the comprehensive index (*CI*), which was defined based on partially annotated voxel-level ground truth. Finally, the performance of the proposed H-CNN was tested by the *CI* values as well as visual inspection via curved planar reformation (CPR). To the best of our knowledge, this is the first time the semi-supervised CNN-based method being adopted to cerebrovascular segmentation. The main contributions of this paper are summarized as below:

1) The proposed H-CNN reduces the exquisite model and feature design of rule-based methods into solving the mapping between MRA images (input) and cerebral vessels (output) by semi-supervised learning, which alleviates the dependence on user's domain knowledge.

2) Given the tube-level labels (generated by centerlines and estimated radii), the proposed H-CNN accomplishes the voxel-level vessel segmentation via the hierarchical update of CNN. The reason is that CNN in each iteration of the H-CNN absorbs the learning experience of the previous iteration, which gradually turns a semi-supervised task into a supervised one.

3) To stop the hierarchical update of CNN, we defined the *CI* which integrates six modified quantification indices. The calculation of each index only requires partially the annotated voxel-level ground truth, saving the time spending on the annotation of complete cerebral vasculature.

4) The *CI* and the six modified indices are also employed for the evaluation of the H-CNN in the testing stage. To remove the limitations of these indices on vessels outside the voxel-label ground truth, we visually inspected the segmentation via CPR. The joint quantification evaluation and visual inspection guarantee the rational estimation of segmentation performance.

The rest of this paper is organized as follows. Section II presents the proposed semi-supervised cerebrovascular segmentation method by H-CNN, followed by the experimental results of the proposed method in Section III. The discussions and conclusion are given in Section IV.

## II. METHOD

The framework of the proposed semi-supervised cerebrovascular segmentation method is shown in Fig. 1. Firstly, we generated the tube-level labels of cerebral vessels by given centerlines and estimated radii (section II.A). Secondly, we constructed and trained an H-CNN with the training MRA images and the tube-level labels (section II.B). Thirdly, the stopping criterion used for validation of the H-CNN is defined by the *CI*, which compares the difference between partially

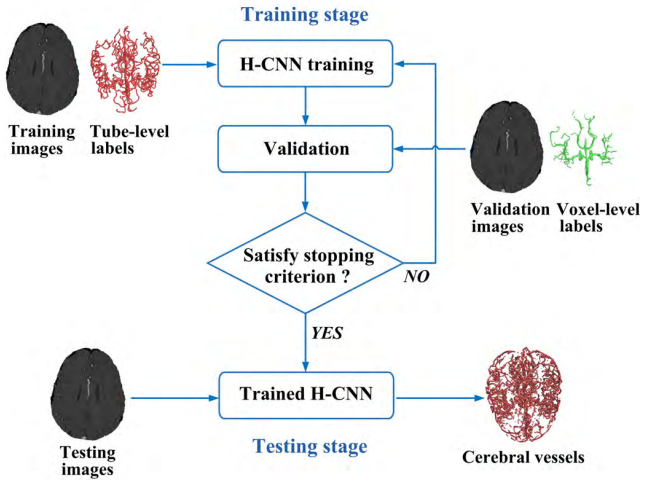


**FIGURE 1.** The framework of the proposed cerebrovascular segmentation method by hierarchical convolutional neural network (H-CNN).

annotated voxel-level ground truth and the prediction on validation images (section II.C). The training (section II.B) and validation (section II.C) of the H-CNN are conducted alternately until the stopping criterion is satisfied. Lastly in the testing stage, we fed the trained H-CNN with testing MRA images and obtained the segmented cerebral blood vessels (section II.D). Because both the tube-level labels and voxel-levels labels are involved in the training stage, the proposed H-CNN is essentially a semi-supervised method.

### A. TUBE-LEVEL LABEL GENERATING

Since H-CNN belongs to a semi-supervised learning method, it is necessary to partially label the vessels on the original MRA images. Unfortunately, manually labeling of cerebral vessels has turned out to be laborious and erroneous on thin vessels. Therefore, based on the tubular structures of cerebral vessels, we attempted to reconstruct our tube-level labels with vessel centerlines and estimated radii. Compared with the pixel-wise annotation by voxel-level labels, the tube-level labels only coarsely annotate the cerebrovascular regions confined by the estimated radii. Therefore, these tube-level labels are essentially weak labels.

Centerlines are generally used to simplify the representation and measure the morphological parameters of blood vessels [48]. There are numerous automatic centerline extraction methods, which facilitate the centerline acquisition from original images. There are several ways to generate blood vessels model using centerlines. Mendonca and Campilho [49] used centerlines to guide an iterative region growing method and obtained the final segmentation. The region growing method integrates the contents of several binary images resulting from vessel width dependent morphological filters. Lell *et al.* identified the lumen boundary on orthogonal cross-sectional images and found the cross-sectional measurement. The cross-sectional measurement diagram represents the diameter of the selected vessel segment [50].

In this paper, we reconstructed the tube-level labels of cerebral vessels by moving spheres centered at the centerline points with estimated radii. In detail, we compared the Euclidean distance of each voxel on MRA images from the current centerline point with the corresponding radius. If the Euclidean distance was less than corresponding radius, we labeled this voxel as blood vessels. Otherwise, we labeled this point as the background.

The generated tube-level labels were actually not accurate due to the following two reasons. Firstly, some of the given centerline points were slightly deviated from the real center of blood vessels. Worse yet, the centerlines were often missing especially on thin cerebral vessels. Secondly, the reconstructed blood vessels did not completely overlap the real ones, which was mainly caused by the errors in the estimated radii. These reasons led to the incorrect labels of cerebral vessels, which are illustrated in Fig.2. It shows that some vessel voxels were labeled as the background, which might lead to under-segmentation (white arrow). On the other hand, some background voxels were incorrectly labeled as vessels that might lead to over-segmentation (red arrow). In this sense, the tube-level labels just provided approximate locations of cerebral vessels.

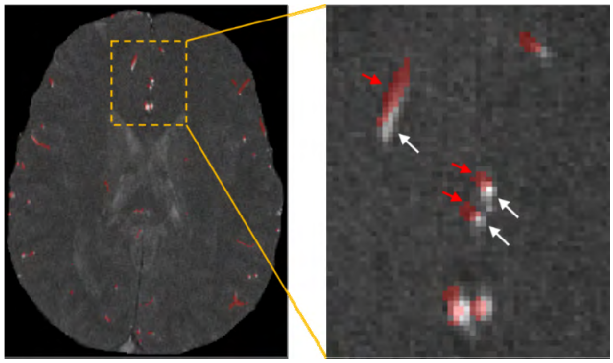

**FIGURE 2.** Incorrect tube-level labels of cerebral vessels. The red arrows indicate the cases that the background were labeled as vessels; and the white arrows indicate the cases that vessels were labeled as the background.

### B. HIERARCHICAL CONVOLUTIONAL NEURAL NETWORKS (H-CNN)

As one of state-of-the-art machine learning algorithms, convolutional neural networks (CNNs) can directly learn features from input images and avoid the complex handcrafted feature extraction compared with traditional machine learning method. Therefore, more and more CNNs have been adopted in medical image processing in recent years. Specifically, Kamnitsas *et al.* [51] proposed a 3D CNN for medical image processing, which performed well in three challenging tasks of lesion segmentation with complete labels. However, existing CNNs are seldom used as weak- or semi-supervised learning method for medical image segmentation. In this paper, we segmented cerebral vessels with an H-CNN in a semi-supervised way. Fed with the training MRA images and the tube-level labels, the proposed H-CNN accomplished the voxel-level segmentation of cerebral vessels via the hierarchical update of CNN.

The structure of the proposed H-CNN is shown in Fig 3. In each iteration, we trained a CNN with the training images and updated labels. The architecture of our CNN is based on the 3D CNN proposed by Kamnitsas *et al.* [51], because it has the ability to segment brain lesions with extremely high accuracy. After the training, we validated the trained CNN by comparing the prediction on the validation images with the partially annotated voxel-level labels (see II.C), and determined whether the stopping criterion is satisfied. If not, we would continue the training of CNN in the next iteration using the same training images but with updated labels that merged the input and output labels of the last iteration.

The implementation details of the H-CNN are described as follows. On the $i^{\text{th}}$ iteration, we trained the CNN by the training images (T-images) and the updated labels by the last iteration, denoted by $l_{i-1}^{N}$, where the initial labels in the first iteration were actually the generated tube-level

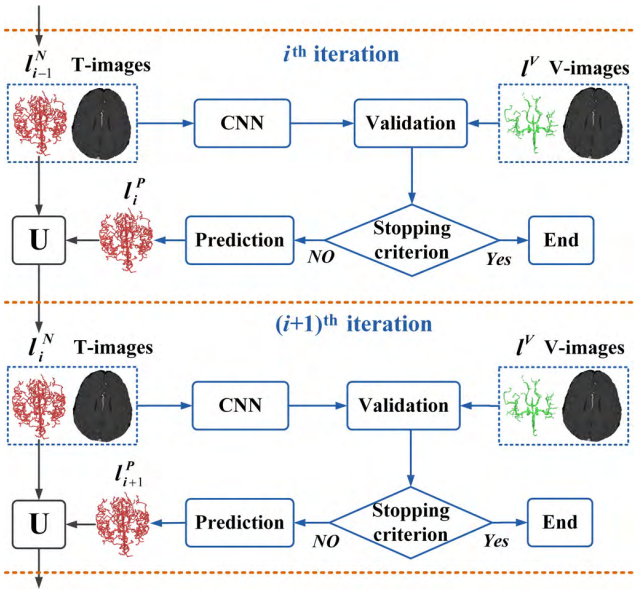


**FIGURE 3.** Training of the proposed hierarchical convolutional neural network (H-CNN). T-images is the abbreviation of trainings images. V-images is the abbreviation of validation images. $I^V$ is the voxel-level labels of validation images.

labels. Then, we validated the trained CNN on the validation images (V-images) by calculating the comprehensive index (*CI*) (Section II.C), which compared the predictions on V-images with the voxel-level labels. If *CI* value was not less than a given threshold, we would stop the update of the H-CNN. Otherwise, we would use the trained CNN to predict training images (T-images), and obtain the predicted labels, denoted by $l_i^P$. The update of labels in this iteration is given by Eq. (1), which subsequently start the hierarchical iteration of the $(i+1)^{\text{th}}$ iteration.

$$l_i^N = l_i^p \cup l_{i-1}^N \tag{1}$$

We used the cross entropy as the cost function in the $(i+1)^{\text{th}}$ iteration,

$$C^{i+1}(\phi^{i+1}; I, l_i^N) = -\frac{1}{B}\sum_{j=1}^{B}\log(P(l_{i+1}^P = l_i^N | I^j, \phi^{i+1})) + \partial||w||_1 + \beta||w||_2^2 \tag{2}$$

where $\phi^{i+1}$ is the parameters of CNN in the $(i+1)^{\text{th}}$ iteration, $(I^j, l_i^N)$ is the $j^{\text{th}}$ patch in the batch and the corresponding labels of the $(i+1)^{\text{th}}$ iteration, $B$ is the batch size that controls the sample size in the training stage in each iteration, $P(l_{i+1}^P = l_i^N | I^j, \phi^{i+1})$ is the predicted posterior probability for $I^j$, $\partial||w||_1$ and $\beta||w||_2^2$ can avoid the problem of overfitting, which balance the requirement of sparsity and robustness, respectively. We also adopted two parallel convolutional pathways in our H-CNN, which could learn the features of cerebral blood vessels at multi-scales. The input of the first pathway had the same central voxels as the second pathway, but it was a down-sampling of the bigger patches on the first pathway with the factor $\alpha$. In this paper, we set $\alpha$ as 3, which balanced the trade-off between accuracy and computation capacity.

Although the parallel convolutional pathways were employed in the proposed H-CNN, it is still a voxel-wise classification that often lead to the problem of isolated points. There may be several cerebrovascular points in the background region, or several background points in the cerebrovascular region. Conditional random field (CRF) is a statistical model that takes arbitrary context into account. Specifically, it considers the regional information of input images in its energy function, thus has great potential to solve the above problem. Therefore, we employed the fully connected CRF as the post-processing of the H-CNN [52]. In the fully connected pairwise CRF model, the Gibbs energy of an input image $I$ is given as follows,

$$E(l) = \sum_m \varphi_u(l_m) + \sum_{m,n,m\neq n} \varphi_c(l_m, l_n) \tag{3}$$

The first term is the sum of the unary potential $\varphi_u(l_m) = -\log P(l_m|I)$, where $P(l_m|I)$ is the output of the H-CNN for voxel $m$. The unary potential represents the regional energy. The higher the probability of a voxel belongs to vessels, the more likely the voxel is classified as cerebral vessels. The second term is the sum of pairwise potential for voxels $m$ and $n$,

$$\varphi_c(l_m, l_n) = \mu(l_m, l_n)\left[w_1 \exp\left(-\sum_{d=\{x,yz\}}, \frac{|p_{m,d}-p_{n,d}|^2}{2\sigma_\gamma^2}\right) + w_2 \exp\left(-\sum_{d=\{x,yz\}}, \frac{|p_{m,d}-p_{n,d}|^2}{2\sigma_\beta^2}\frac{|I_m-I_n|^2}{2\sigma_\alpha^2}\right)\right] \tag{4}$$

where the $w_1$-weighted part is the smoothness function for removing small isolated regions, in which the extent of smoothness are controlled by the parameter $\sigma_\gamma$. The $w_2$-weighted part is the appearance function that classifies the voxel with similar intensity and small distance as the same class, in which the extent of nearness and similarity are controlled by parameters $\sigma_\beta$ and $\sigma_\alpha$, respectively. $p_{m,d}$ and $p_{n,d}$ are the voxel coordinates in the feature space, $I_m$ and $I_n$ are the intensities, $\mu(l_m, l_n)$ is the Heaviside step function,

$$\mu(l_m, l_n) = \begin{cases} 1 & l_m \neq l_n \\ 0 & l_m = l_n \end{cases} \tag{5}$$

The pairwise potential represents the boundary energy. Under the effect of Heaviside step function, the boundary energy only considers the case that two voxels are segmented into two different classes. The more distant two voxels are in feature space and the more distinct the two voxels are in intensities, the more likely that the two voxels are classified as different objects (i.e. vessels and the background).

### C. STOPPING CRITERION

With the increase of iterations, the updated labels cover more and more voxels that belong to vessels with high probability.

The increased labels can also alleviate the data imbalance between vessels and background. However, excessive iterations may contribute little for improving the accuracy, and may also lead to the dramatic increase of computation time. Therefore, the critical problem is to find the stopping criterion in validation, so as to terminate the hierarchical update of the H-CNN. Most of the quantification indices require the entire cerebral vasculature as the ground truth. However, some cerebral vessels are complex and thin in morphology, it is troublesome to annotate the entire blood vessels. Therefore, we manually annotated partial vessels near the circle of Willis as the voxel-level ground truth. In order to guarantee the robustness and accuracy of the ground truth, the manual annotation of the voxel-level labels obeyed the following guidelines:

(1) The annotation should be initialized in the two dimensional (2D) section of MRA images that includes the center position of the circle of Wills;

(2) The annotation must be continuous and gradually grow along the above and below sections from the section of initial annotation. During the growing, both the large and small blood vessels are recruited. If there is a bifurcation, all the branches starting from this bifurcation must be tracked;

(3) The annotation is terminated when all the branches have been fully tracked. The meaning of ''fully tracked'' is that each branch of the circle of Wills grows until the difference between vessels and the background disappears.

Based on the voxel-level ground truth, we defined the comprehensive index (*CI*) to stop the update of hierarchy, which integrates six modified quantification indices. Four indices are based on the difference between segmented vessels and ground truth vessels, including sensitivity, specificity, accuracy, and Hausdorff distance. Two evaluation indices are based on vessel centerlines, including radius error and the number of centerline points.

The ground truth positive samples were the voxel-level cerebral vessels. However, the ground truth negative samples were not the supplementary set of the ground truth positive samples. In other words, we must remove the voxels belonging to vessels with high probability from this supplementary set. Therefore, we firstly fed the trained H-CNN with the MRA images and predicted the cerebral vessels; Then, we conducted the vesselness filtering [7] to enhance the MRA images and segmented the cerebral vessels with proper threshold. Finally, we obtained the ground truth negative samples by excluding the predicted cerebral vessels and vesselness filter segmentation from the above supplementary set. Based on the ground truth positive and negative samples, the sensitivity, specificity, and accuracy are defined as,

$$SEN = \frac{TP}{TP + FN} \tag{6}$$

$$SPC = \frac{TN}{TN + FP} \tag{7}$$

$$ACC = \frac{TP + TN}{TP + TN + FN + FP} \tag{8}$$

where $TP$ is the number of true positive voxels, $FN$ is the number of false negative voxels, $TN$ is the number true negative voxels, $FP$ is the number of false positive voxels.

With the voxel-level ground truth, we changed the bidirectional Hausdorff distance to the unidirectional Hausdorff distance, i.e. the distance from the manually annotated voxel-level ground truth to the segmented cerebral blood vessels,

$$d_H = \frac{1}{N} \sum \{\sup_{x \in X} \inf_{y \in Y} d(x, y)\} \tag{9}$$

where $\sup(\cdot)$ and $\inf(\cdot)$ represent the supremum and the infimum respectively, $X$ is the set of ground truth positive samples, and $Y$ is the set of segmented cerebral vessels.

The first index based on vessel centerlines is the number of centerline points of segmented cerebral blood vessels,

$$N_{CP} = \|C\|_0 \tag{10}$$

where $C$ is the vector of centerline points, and $N_{CP}$ is the $l_0$-norm (element number) of $C$. The value of $N_{CP}$ for correct segmentation is generally larger than that of under segmentation, with the premise that the centerlines in both cases are continuous.

The second index is the radius error, which compares the given estimated radius with the predicted one based on centerline by the following equation:

$$d_R = \frac{1}{M} \sum_{x \in C_X, y \in C_Y} |R(y) - R(x)| \tag{11}$$

where $R(x)$ is the radius of point $x$ on the original centerline $C_X$, which is chosen as the reference. $R(y)$ is the radius of centerline point $y$ on the segmented centerline $C_Y$. The value of $R(y)$ is calculated as the radius of the minimum inscribed circle within the segmented vessels by H-CNN. To establish the correspondence between the two centerlines $C_X$ and $C_Y$, $y$ is the closest centerline point away from $x$ (i.e. the paired centerline point of $x$).

Until now, we have presented six indices to quantify the segmentation, including the sensitivity (*SEN*), specificity (*SPC*), accuracy (*ACC*), Hausdorff distance ($d_H$), number of centerline points ($N_{CP}$) and radius error ($d_R$). However, different evaluation indices may have contradictory suggestion when making stopping determination of the hierarchical update of the H-CNN. Therefore, we proposed the comprehensive index (*CI*) based on the six evaluation indices, defined by the following equation,

$$CI = ACC + SEN + SPC - \frac{1}{4}(d_H + d_R) + \frac{1}{10}\log_{10} N_{CP} \tag{12}$$

The larger the *CI* value is, the more accurate segmentation we can obtain by the proposed H-CNN. Therefore, we reduced finding the stopping criterion to the evaluation of *CI*, so as to determine the best hierarchy of the H-CNN. In detail, if *CI* value was not less than $\varepsilon$ (the empirically value of $\varepsilon$ was set as 2.95), we would stop the update of the hierarchy and obtain the optimal H-CNN for cerebrovascular segmentation.

### D. TESTING STAGE

Based on the hierarchical training and validation with the stopping criterion, we finally obtained the optimal H-CNN. For new brain MRI images, we fed them to the trained H-CNN and classified each voxel as cerebral vessels or the background. Since the voxel-wise classification leads to the issue of isolated points, we used the fully connected CRF as the post-processing procedure to obtain the final segmentation of cerebral vessels. Based on the partially annotated voxel-level ground truth, we also utilized the comprehensive index (*CI*) as well as the visual inspection by curved planar reformation (CPR) to evaluate the performance of segmentation in the experiment (section III).

## III. EXPERIMENTS AND RESULTS

The experimental data we used were the designed database of MR images of healthy volunteers from MIDAS platform [53]. Except for the original brain MRA images, these data also include vessel centerlines and estimated radii. In this section, we firstly pre-processed the MRA images and generated the tube-level labels of cerebral vessels. Secondly, we discussed the tuning of H-CNN hyper-parameters, followed by the validation of the H-CNN at different hierarchies. Finally, we showed the results of H-CNN and the comparison with other methods.

### A. PRE-PROCESSING

The MRA image of skulls generally has the similar shape information compared with the cerebral vessels. Thus, we manually removed skulls from all the brain images with the guidance of specialists. On the other hand, all the images were normalized as the standard data with zero-means and unit-variances. The normalization facilitated the subsequent training of the H-CNN. Based on the given vessel centerlines and radii, we reconstructed the cerebral vessels with the tube-level label generating method (section II.A). Then, we randomly partitioned the processed data into three subsets including training, validation and testing datasets. Partial voxel-level ground truth vessels used for validation and testing were manually annotated by experienced specialists. We used 20 training data to train our H-CNN and tried to explore the optimal iteration with the stopping criterion on different number of validation data (1-6), and finally obtained the results and evaluated the H-CNN on the 6 testing data.

### B. HYPER-PARAMETER TUNING

The basic CNN on each iteration of the H-CNN had the same architecture including convolution, pooling, and active functions. Therefore, it was necessary to tune the network hyper-parameters to make the CNN suitable for our task of cerebrovascular segmentation. Therefore, we fed the basic CNN with the training dataset and adjusted the two important hyper-parameters: epoch and the decreasing way of the learning rate. Then we input 3 validation data to the trained CNN and calculated the quantification indices. The results of different quantification indices are shown in Table 1.

**TABLE 1. Tuning of the basic CNN with different epochs and the decreasing way of the learning rate.**

| | Epo | *SEN* (%) | *SPC* (%) | *ACC* (%) | $d_H$ (pix) | $d_R$ (pix) | $N_{CP}$ ($10^4$) | *CI* |
|---|---|---|---|---|---|---|---|---|
| Q | 20 | 70.36 | **100** | 87.69 | 0.61 | 0.98 | **1.22** | 2.58 |
| | 35 | 72.13 | **100** | 87.60 | 0.61 | 0.89 | **1.22** | 2.63 |
| | 50 | 72.50 | **100** | 87.76 | 0.61 | 0.91 | 1.17 | 2.63 |
| E | 20 | **73.29** | **100** | **88.10** | **0.60** | 0.90 | 1.20 | **2.65** |
| | 35 | 72.70 | **100** | 87.86 | 0.61 | 0.90 | **1.22** | 2.63 |
| | 50 | 72.69 | 99.99 | 87.85 | 0.62 | **0.87** | 1.20 | 2.64 |

Note: Q and E stand for quadratic and exponential, respectively. Epo represents different epochs.

The exponential decease of learning rate performed better in terms of*SEN*and*ACC*, and comparably in terms of*SPC*, $d_H$, $d_R$, and $N_{CP}$. This led to the higher *CI* of the exponential decease of learning rate than the quadratic one. One the other hand, it was observed that different epochs had influence on the segmentation performance. When epoch value equaled 20, the indices *SEN*, *ACC*, and $d_H$ were slightly better than the other epoch values, resulting in the higher value of *CI*. Therefore, the recommended combination of these two hyper-parameters was the exponential decease of learning rate and the epoch equals 20.

### C. VALIDATION OF THE H-CNN

In each iteration, we trained the CNN with the updated labels and then predicted the cerebral blood vessels on validation data. The results in one of the MRA images at different iterations (1$^{st}$, 5$^{th}$, 10$^{th}$, and 15$^{th}$) are shown in Fig. 4. In the 2D results, we noticed more and more cerebral blood vessels were correctly segmented with the increase of iterations. Specifically, the connectivity of vessels was improved (see the white arrows in the first row of Fig. 4). The similar trend could also be found in the 3D visualization of the segmented cerebral vessels. We further showed the 3D overlap between the predicted vessels (red) and the manually annotated voxel-level ground truth (green) in the last row of Fig. 4. In the first iteration, most of the green vessels were uncovered by the red vessels indicating the existence of under-segmentation. Along the hierarchical iteration, the overlapped ratio between the segmented vessels and the ground truth was increasing. The results visually demonstrated that the H-CNN in higher iterations could segment more cerebral vessels.

We also quantitatively validated the H-CNN in each iteration with different numbers of validation data, so that we could determine whether the stopping criterion was robust. The quantitative validation on six individual indices are shown in Fig. 5. Among the six indices, the *SEN* rose dramatically and then slowly with the increase of iterations, which indicated more and more true vessels were successfully segmented. The *SPC* slightly decreased in higher iterations, meaning that the recognition of true background was nearly

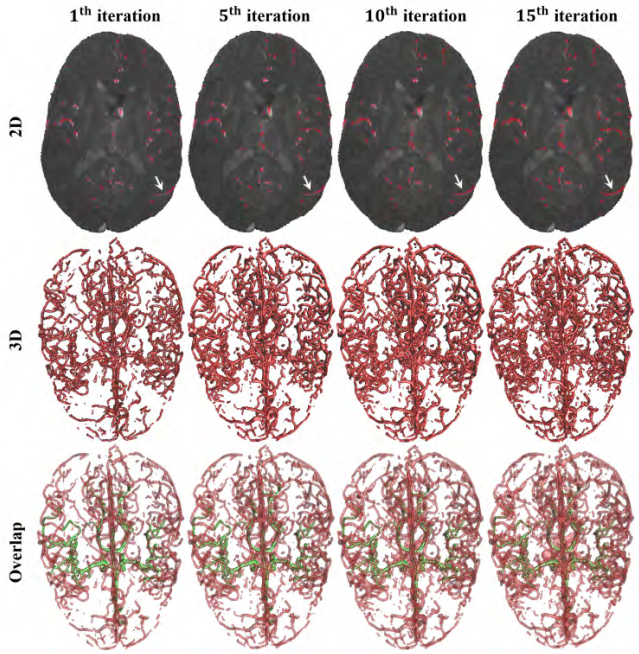


**FIGURE 4.** Results of segmented cerebral vessels by the H-CNNs in different iterations. The 2D, 3D and the 3D overlap with ground truth are shown in the first, second and third rows, respectively, where the ground truth are colored green. The insets from the left to right columns are the results of the H-CNN in the 1st, 5th, 10th, and 15th iteration, respectively.

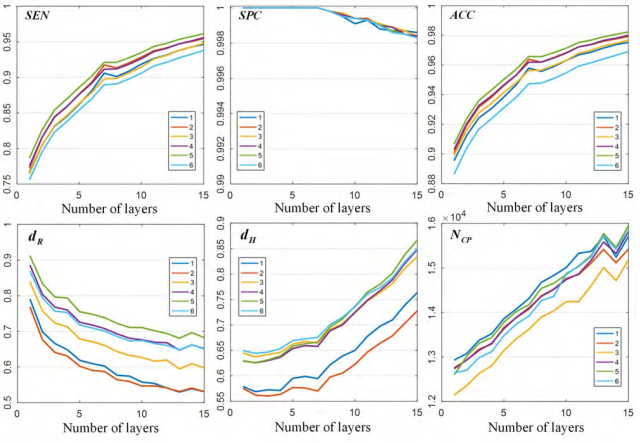


**FIGURE 5.** Validation results of six individual quantification indices in different iterations with different numbers of validation data.

iteration-irrelevant. Combining the *SEN* and *SPC*, the*ACC* had the similar trend with *SEN*, increasing from 89.91% to 97.68% when 3 validation data were used. The radius error $d_R$ decreased dramatically and then slowly with the increase of iterations, while the Hausdorff distance $d_H$ had slow increase. $N_{CP}$ was incremental from 1st to the 13th iteration, indicating more and more vessels were segmented from the MRA images. In Fig. 6, we showed the centerlines of the corresponding segmented cerebral vessels. It was observed that the connectivity of the centerline was improved. Therefore,

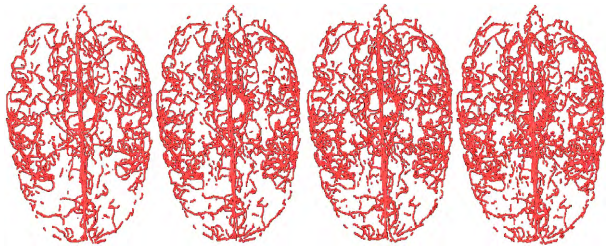

**FIGURE 6.** Results of extracted centerlines of segmented vessels by the H-CNNs in different iterations. The insets from the left to ri6ght columns are the centerlines of the H-CNN in 1st, 5th, 10th and 13th iteration respectively.

the $N_{CP}$ was a good indication of the number of correct cerebral vessels.

The values of each index fluctuated slightly when different numbers of validation data were used. Nevertheless, the similar trend could be found in each individual index with the increase of iterations, which demonstrated the determination of stopping criterion was irrelevant to the number of validation data. The similar trend could be found in Table 2. Integrating all the six individual indices, the highest *CI* values of 1, 2, 5 and 6 validation data were found in the 13th iteration of the H-CNN. The highest *CI*values of 3 and 4 validation data were found at both the 13th and 14th iterations. The validation experiment demonstrated the optimal architecture for the cerebrovascular segmentation was the H-CNN with 13 iterations.

**TABLE 2.** Validation of the H-CNN with different numbers of validation MRA images at different iterations using the comprehensive index (*CI*).

| | 1datum | 2 data | 3 data | 4 data | 5 data | 6 data |
|---|---|---|---|---|---|---|
| 1 | 2.73 | 2.75 | 2.70 | 2.71 | 2.72 | 2.67 |
| 2 | 2.81 | 2.84 | 2.78 | 2.79 | 2.80 | 2.75 |
| 3 | 2.86 | 2.89 | 2.83 | 2.84 | 2.85 | 2.80 |
| 4 | 2.88 | 2.91 | 2.85 | 2.86 | 2.87 | 2.82 |
| 5 | 2.91 | 2.94 | 2.88 | 2.89 | 2.90 | 2.85 |
| 6 | 2.94 | 2.97 | 2.90 | 2.91 | 2.92 | 2.88 |
| 7 | 2.98 | 3.01 | 2.94 | 2.94 | 2.95 | 2.91 |
| 8 | 2.97 | 3.00 | 2.94 | 2.94 | 2.95 | 2.91 |
| 9 | 2.98 | 3.01 | 2.95 | 2.95 | 2.96 | 2.92 |
| 10 | 3.00 | 3.02 | 2.96 | 2.96 | 2.96 | 2.93 |
| 11 | 3.00 | 3.03 | 2.97 | 2.97 | 2.97 | 2.94 |
| 12 | 3.01 | 3.03 | 2.97 | 2.97 | 2.97 | 2.94 |
| 13 | **3.02** | **3.04** | **2.98** | **2.98** | **2.98** | **2.95** |
| 14 | 3.01 | 3.03 | **2.98** | **2.98** | 2.97 | 2.94 |
| 15 | 3.01 | 3.03 | 2.97 | 2.97 | 2.97 | 2.94 |

### D. RESULTS AND COMPARISON

In this experiment, we compared the proposed H-CNN with the other segmentation methods, including the vesselness filtering (vesselness) [7], bi-Gaussian curvilinear filtering (bi-Gauss) [54], optimally oriented flux (OOF) [55], vessel enhanced diffusion (VED) [10], hybrid diffusion with continuous switch (HDCS) [16], Mimics software (https://www.materialise.com/en/medical/software/mimics), 2D CNN ($CNN_{2D}$) [47], and 3D CNN ($CNN_{3D}$) [51].

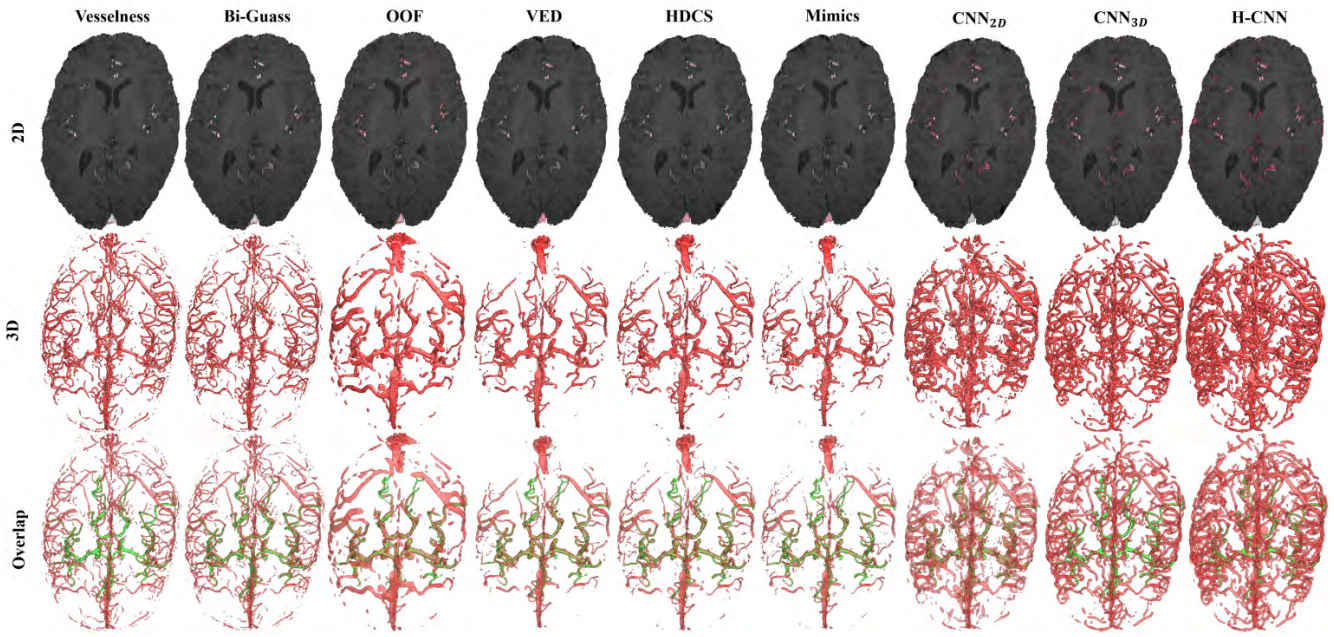


**FIGURE 7.** Results of segmented cerebral vessels by different methods. The insets from the left to right columns are the results of vesselness filtering (vesselness), bi-Gaussian curvilinear filtering (bi-Gauss), optimally oriented flux (OOF), vessel enhanced diffusion (VED), hybrid diffusion with continuous switch (HDCS), Mimics software $CNN_{2D}$, $CNN_{3D}$, and H-CNN, respectively.

The comparison was conducted on the six testing MR images, whose results are given in Fig. 7. Since the vesselness and bi-Gauss were essentially image enhancement methods, different thresholds were tried to segment the enhanced cerebral vessels. The segmented results with the optimal thresholds (from ROC curves) are shown as the first and second columns of Fig. 7. Obviously, these two filtering methods could only segment the main vessels, or the vessels that have distinct intensity difference from the background. From the third column of Fig. 7, we observed that the OOF tended to over-segment the main vessels, while all the thin vessels were missing. Compared with the above three methods, the VED, HDCS, and Mimics finely delineated the large vessels near the manually labeled ground truth vessels (the fourth to sixth columns). Nevertheless, a great proportion of vessels located way from the circle of Willis were under-segmented. The results of both the $CNN_{2D}$ and $CNN_{3D}$ demonstrated the ability of deep learning for segmenting cerebral blood vessels (the seventh and eighth columns). However, a great proportion of cerebral vessels failed to be fully segmented due to the problem of inaccurate tube-level labels. This imperfect segmentation was greatly improved with the proposed H-CNN (the last column). We also showed the overlapped results between each method and the manually labeled voxel-level ground truth in the last row of Fig.7. Nearly all the true vessels near the circle of Willis were covered by the H-CNN segmented vessels.

The six individual indices (*SEN*,*SPC*,*ACC*, $d_H$, $d_R$ and $N_{CP}$) and the comprehensive index (*CI*) were also utilized for the quantitative estimation of different methods in Table 3. We found H-CNN ranked the first in terms of*SEN*, *ACC*, $d_R$, $N_{CP}$, as well as *CI*. Specifically, the index *SEN* showed the superiority of the proposed H-CNN over the other eight methods, which was 66.42, 64.00, 66.05, 91.41, 90.43, 90.48, 91.40, 77.52, and 94.69% for vesselness, bi-Gauss, OOF, VED, HDCS, Mimics, $CNN_{2D}$, $CNN_{3D}$, and H-CNN, respectively. This demonstrated that H-CNN had the excellent ability for recognizing cerebral blood vessels even though the tube-level labels were incomplete. The*CI* of H-CNN (2.99) ranked the first among the nine methods, which indicated the segmented cerebral vessels had high overlapping ratio with the partial manually annotated voxel-level ground truth.

**TABLE 3.** Quantitative comparison of the proposed H-CNN with other segmentation methods.

| | *SEN* (%) | *SPC* (%) | *ACC* (%) | $d_H$ (pix) | $d_R$ (pix) | $N_{CP}$ ($10^4$) | *CI* |
|---|---|---|---|---|---|---|---|
| **Vesselness** | 66.42 | **100** | 84.16 | **0.45** | 3.39 | 0.88 | 1.94 |
| **Bi-Gauss** | 64.00 | 99.93 | 84.04 | 0.61 | 3.12 | 0.95 | 1.95 |
| **OOF** | 66.05 | 99.77 | 82.92 | 2.51 | 9.68 | 0.51 | -0.19 |
| **VED** | 91.41 | 99.93 | 96.41 | 0.55 | 5.57 | 0.60 | 1.73 |
| **HDCS** | 90.43 | 99.92 | 96.22 | 0.49 | 4.27 | 0.68 | 2.06 |
| **Mimics** | 90.48 | 99.94 | 96.85 | 0.48 | 4.31 | 0.62 | 2.05 |
| **$CNN_{2D}$** | 91.40 | 99.80 | 95.30 | 0.70 | 1.25 | 1.32 | 2.79 |
| **$CNN_{3D}$** | 77.52 | **100** | 90.57 | 0.65 | 0.87 | 1.26 | 2.71 |
| **H-CNN** | **94.69** | 99.86 | **97.85** | 0.79 | **0.64** | **1.57** | **2.99** |

In order to estimate the segmentation of H-CNN outside the partially annotated ground truth, we transformed MRA images and segmented the thin vessels from three orthogonal view to the curved planar reformation (CPR) view (Fig. 8). In longitudinal observation, we found a majority of the thin cerebral vessels were correctly segmented by H-CNN (Fig. 8(a)-(c)). Then, we tried our best to find six local vessels

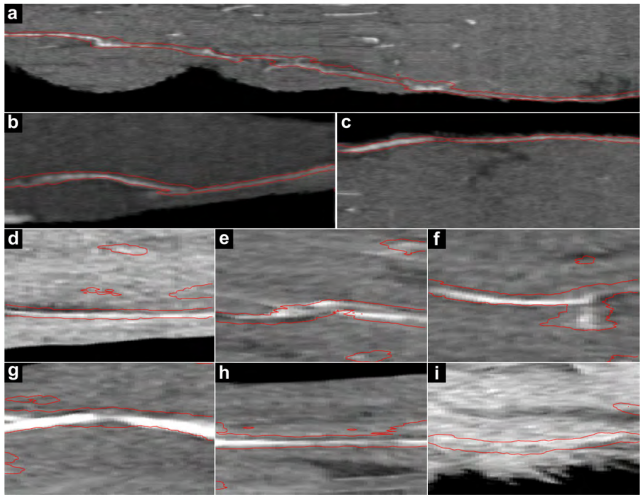


**FIGURE 8.** Curved planar reformation (CPR) view of segmented cerebral vessels by H-CNN outside the partially annotated ground truth. (a)-(c) Three segmented vessels in longitudinal observation. (d)-(i) Six poorly segmented vessels in local observation.

that were not fully segmented (Fig. 8(d)-(i)). Even though slight over-segmentation could be observed in Fig. 8(d)-(h), most part of these vessels were successfully segmented. The correctness of the segmentation in Fig. 8(i) was unknown due to the similar intensity with the background, which requires further investigation.

## IV. DISCUSSION AND CONCLUSION

The quantification analysis demonstrated that the proposed H-CNN outperformed the $CNN_{2D}$ proposed by Phellan *et al* [47], and the $CNN_{3D}$ proposed by Konstantinos *et al*. [51], even though the tube-level labels of vessels were neither complete nor accurate. The reason is that H-CNN allows the update of labels in each iteration. Therefore, the segmentation is gradually improved with the increase of iterations. Nevertheless, some of the updated labels may incorrectly treat a few background voxels as vessels. In fact, this problem is actually not worth worrying about, because the learning of background voxels in positive samples is far less than the learning of the background voxels in negative samples. Therefore, the over-segmentation of H-CNN resulting from this problem is negligible, which can be affirmed by the slightly decrease of specificity (*SPC*) in Fig. 5. Generally, H-CNN uses more time for hierarchical training compared with CNN, because the former improves the accuracy of cerebrovascular segmentation at the expense of training time.

Among the six indices in the stopping criterion, the sensitivity (*SEN*) and *SPC* indicate the problem of under- and over-segmentation, respectively. In other words, the occurring of under- or over-segmentation will decrease the value of *SEN* or *SPC*, respectively. The accuracy (*ACC*), Hausdorff distance ($d_H$), and radius error ($d_R$) represent the overall accuracy of segmentation. No matter under- or over-segmentation occurs, the value of *ACC* will decrease, while the values of $d_H$ and $d_R$ will increase. The utilization of numbers of centerline points ($N_{CP}$) must be guided by the visualization of centerlines. When the centerline has good connectivity, higher value of $N_{CP}$ indicates the improvement of under-segmentation. However, when the centerline is fractured, $N_{CP}$ fails to be used as the quantification index, because the over-segmentation in this case may also lead to a higher value of $N_{CP}$. The proposed comprehensive index (*CI*) integrates all the six indices with relatively equal weights, which balances the contradictions among different indices. The *CI* value has great consistency with the visual inspection when used in the stopping criterion and quantitative evaluation of different methods.

In conclusion, we proposed a semi-supervised cerebrovascular segmentation method with a hierarchical convolutional neural network (H-CNN). We firstly generated inaccurate tube-level labels of vessels with the given centerlines and radii. Secondly, we constructed and trained the H-CNN with the training MRA images and corresponding tube-level labels. Thirdly, we validated the H-CNN with the stopping criterion, i.e. the comprehensive index (*CI*), which integrated six individual quantification indices. The quantification indices took the partially annotated voxel-level labels near the circle of Willis as the ground truth, saving the time spending on the annotation of complete cerebral vasculature. Finally, the performance of the proposed H-CNN was tested by the quantification indices as well as visual inspection via curved planar reformation (CPR). The experimental results demonstrated that the proposed H-CNN greatly improved the segmentation of cerebral blood vessels, even though the tube-level labels were incomplete and not totally correct. The proposed H-CNN can facilitate accurate diagnosis of cerebrovascular diseases, which can also be used in other medical image segmentation with only weak and partially correct labels.

## ACKNOWLEDGMENT

The authors also would like to thank Dr. Muhan Liu for his assistance in polishing the manuscript. The MR brain images from healthy volunteers used in this paper were collected and made available by the CASILab at The University of North Carolina at Chapel Hill and were distributed by the MIDAS Data Server at Kitware, Inc.

## REFERENCES

[1] M. Park, B. Kang, S. J. Jin, and S. Luo, "Computer aided diagnosis system of medical images using incremental learning method," *Expert Syst. Appl.*, vol. 36, no. 3, pp. 7242–7251, Apr. 2009.

[2] M. Yasugi, B. Hossain, M. Nii, and S. Kobashi, "Relationship between cerebral aneurysm development and cerebral artery shape," *J. Adv. Comput. Intell. Inform.*, vol. 22, no. 2, pp. 249–255, 2018.

[3] Z. Watanabe, N. Tomura, I. Akasu, R. Munakata, K. Horiuchi, and K. Watanabe, "Comparison of rates of growth between unruptured and ruptured aneurysms using magnetic resonance angiography," *J. Stroke Cerebrovascular Diseases*, vol. 26, no. 12, pp. 2849–2854, Dec. 2017.

[4] O. Al-Kwifi, D. J. Emery, and A. H. Wilman, "Vessel contrast at three Tesla in time-of-flight magnetic resonance angiography of the intracranial and carotid arteries," *Magn. Reson. Imag.*, vol. 20, no. 2, pp. 181–187, Feb. 2002.

[5] A. Ajam, A. A. Aziz, V. S. Asirvadam, A. S. Muda, I. Faye, and S. J. S. Gardezi, "A review on segmentation and modeling of cerebral vasculature for surgical planning," *IEEE Access*, vol. 5, pp. 15222–15240, 2017.

[6] A. F. Frangi, W. J. Niessen, K. L. Vincken, and M. A. Viergever, "Multiscale vessel enhancement filtering," *Medical Image Computing and Computer-Assisted Intervention—MICCAI*, W. M. Wells, A. Colchester, and S. Delp, Eds. Berlin, Germany: Springer, 1998, pp. 130–137.

[7] Y. Sato *et al.*, "Three-dimensional multi-scale line filter for segmentation and visualization of curvilinear structures in medical images," *Med. Image Anal.*, vol. 2, no. 2, pp. 143–168, 1998.

[8] F. Zhao *et al.*, "Automatic segmentation method for bone and blood vessel in murine hindlimb," *Med. Phys.*, vol. 42, no. 7, pp. 4043–4054, Jul. 2015.

[9] X. Du, H. Ding, W. Zhou, G. Zhang, and G. Wang, "Cerebrovascular segmentation and planning of depth electrode insertion for epilepsy surgery," *Int. J. Comput. Assist. Radiol. Surg.*, vol. 8, no. 6, pp. 905–916, Nov. 2013.

[10] R. Manniesing, M. A. Viergever, and W. J. Niessen, "Vessel enhancing diffusion—A scale space representation of vessel structures," *Med. Image Anal.*, vol. 10, no. 6, pp. 815–825, Dec. 2006.

[11] N. D. Forkert *et al.*, "Fuzzy-based vascular structure enhancement in time-of-flight MRA images for improved segmentation," *Methods Inf. Med.*, vol. 50, no. 1, pp. 74–83, 2011.

[12] D. Babin, A. Pizurica, J. De Vylder, E. Vansteenkiste, and W. Philips, "Brain blood vessel segmentation using line-shaped profiles," *Phys. Med. Biol.*, vol. 58, no. 22, pp. 8041–8061, Nov. 2013.

[13] M. W. Law and A. C. Chung, "Three dimensional curvilinear structure detection using optimally oriented flux," in *Proc. 10th Eur. Conf. Comput. Vis. IV*, Marseille, France, 2008, pp. 368–382.

[14] O. Merveille, H. Talbot, L. Najman, and N. Passat, "Tubular structure filtering by ranking orientation responses of path operators," in *Proc. Comput. Vis. ECCV*, 2014, pp. 203–218.

[15] P. Perona and J. Malik, "Scale-space and edge detection using anisotropic diffusion," *IEEE Trans. Pattern Anal. Mach. Intell.*, vol. 12, no. 7, pp. 629–639, Jul. 1990.

[16] A. M. Mendrik, E.-J. Vonken, A. Rutten, M. A. Viergever, and B. van Ginneken, "Noise reduction in computed tomography scans using 3-D anisotropic hybrid diffusion with continuous switch," *IEEE Trans. Med. Imag.*, vol. 28, no. 10, pp. 1585–1594, Oct. 2009.

[17] P. Soille, *Morphological Image Analysis: Principles and Applications*. New York, NY, USA: Springer-Verlag, 2003.

[18] R. Phellan and N. D. Forkert, "Comparison of vessel enhancement algorithms applied to time-of-flight MRA images for cerebrovascular segmentation," *Med. Phys.*, vol. 44, no. 11, pp. 5901–5915, Nov. 2017.

[19] L. Wen, X. Wang, Z. Wu, M. Zhou, and J. S. Jin, "A novel statistical cerebrovascular segmentation algorithm with particle swarm optimization," *Neurocomputing*, vol. 148, pp. 569–577, Jan. 2015.

[20] D. L. Wilson and J. A. Noble, "An adaptive segmentation algorithm for time-of-flight MRA data," *IEEE Trans. Med. Imag.*, vol. 18, no. 10, pp. 938–945, Oct. 1999.

[21] M. S. Hassouna, A. A. Farag, S. Hushek, and T. Moriarty, "Cerebrovascular segmentation from TOF using stochastic models," *Med. Image Anal.*, vol. 10, no. 1, pp. 2–18, Feb. 2006.

[22] R. Gan, W. C. K. Wong, A. C. S. Chung, and S. C. H. Yu, "Statistical cerebrovascular segmentation in three-dimensional rotational angiography based on maximum intensity projections," *Int. Congr. Ser.*, vol. 1268, pp. 195–200, Jun. 2004.

[23] R.-F. Cao, X.-C. Wang, Z.-K. Wu, M.-Q. Zhou, and X.-Y. Liu, "A parallel Markov cerebrovascular segmentation algorithm based on statistical model," *J. Comput. Sci. Technol.*, vol. 31, no. 2, pp. 400–416, Mar. 2016.

[24] J. T. Hao, M. L. Li, and F. L. Tang, "Adaptive segmentation of cerebrovascular tree in time-of-flight magnetic resonance angiography," *Med. Biol. Eng. Comput.*, vol. 46, no. 1, pp. 75–83, Jan. 2008.

[25] A. C. S. Chung, J. A. Noble, and P. Summers, "Vascular segmentation of phase contrast magnetic resonance angiograms based on statistical mixture modeling and local phase coherence," *IEEE Trans. Med. Imag.*, vol. 23, no. 12, pp. 1490–1507, Dec. 2004.

[26] A. El-Baz, A. Farag, and G. Gimelfarb, "Cerebrovascular segmentation by accurate probabilistic modeling of TOF-MRA images," in *Image Analysis* (Lecture Notes in Computer Science), H. Kalviainen, J. Parkkinen, and A. Kaarna, Eds. Berlin, Germany: Springer, 2005, pp. 1128–1137.

[27] A. El-Baz *et al.*, "Precise segmentation of 3-D magnetic resonance angiography," *IEEE Trans. Biomed. Eng.*, vol. 59, no. 7, pp. 2019–2029, Jul. 2012.

[28] M. Holtzman-Gazit, R. Kimmel, N. Peled, and D. Goldsher, "Segmentation of thin structures in volumetric medical images," *IEEE Trans. Image Process.*, vol. 15, no. 2, pp. 354–363, Feb. 2006.

[29] T. F. Chan and L. A. Vese, "Active contours without edges," *IEEE Trans. Image Process.*, vol. 10, no. 2, pp. 266–277, Feb. 2001.

[30] R. Manniesing, B. K. Velthuis, M. S. van Leeuwen, I. C. van der Schaaf, P. J. van Laar, and W. J. Niessen, "Level set based cerebral vasculature segmentation and diameter quantification in CT angiography," *Med. Image Anal.*, vol. 10, no. 2, pp. 200–214, Apr. 2006.

[31] L. M. Lorigo *et al.*, "CURVES: Curve evolution for vessel segmentation," *Med. Image Anal.*, vol. 5, no. 3, pp. 195–206, 2001.

[32] A. C. Jalba, M. H. F. Wilkinson, and J. B. T. M. Roerdink, "CPM: A deformable model for shape recovery and segmentation based on charged particles," *IEEE Trans. Pattern Anal. Mach. Intell.*, vol. 26, no. 10, pp. 1320–1335, Oct. 2004.

[33] Y. Cheng, X. Hu, J. Wang, Y. Wang, and S. Tamura, "Accurate vessel segmentation with constrained B-snake," *IEEE Trans. image Process.*, vol. 24, no. 8, pp. 2440–2455, Aug. 2015.

[34] F. Zhao, Y. Chen, Y. Hou, and X. He, "Segmentation of blood vessels using rule-based and machine-learning-based methods: A review," *Multimedia Syst.*, Dec. 2017, doi: 10.1007/s00530-017-0580-7.

[35] M. Descoteaux, D. L. Collins, and K. Siddiqi, "A geometric flow for segmenting vasculature in proton-density weighted MRI," *Med. Image Anal.*, vol. 12, no. 4, pp. 497–513, Aug. 2008.

[36] N. D. Forkert *et al.*, "3D cerebrovascular segmentation combining fuzzy vessel enhancement and level-sets with anisotropic energy weights," *Magn. Reson. Imag.*, vol. 31, no. 2, pp. 262–271, Feb. 2013.

[37] P. Lu *et al.*, "A vessel segmentation method for multi-modality angiographic images based on multi-scale filtering and statistical models," *Biomed. Eng. Online*, vol. 15, p. 120, Nov. 2016.

[38] R. Xiao, H. Ding, F. Zhai, T. Zhao, W. Zhou, and G. Wang, "Vascular segmentation of head phase-contrast magnetic resonance angiograms using grayscale and shape features," *Comput. Methods Programs Biomed.*, vol. 142, pp. 157–166, Apr. 2017.

[39] X. Gao, Y. Uchiyama, X. Zhou, T. Hara, T. Asano, and H. Fujita, "A fast and fully automatic method for cerebrovascular segmentation on time-of-flight (TOF) MRA image," *J. Digit. Imag.*, vol. 24, no. 4, pp. 609–625, Aug. 2011.

[40] N. D. Forkert *et al.*, "Automatic correction of gaps in cerebrovascular segmentations extracted from 3D time-of-flight MRA datasets," *Methods Inf. Med.*, vol. 51, no. 5, pp. 415–422, 2012.

[41] H. Molina-Abril and A. F. Frangi, "Topo-geometric filtration scheme for geometric active contours and level sets: Application to cerebrovascular segmentation," in *Medical Image Computing and Computer-Assisted Intervention—MICCAI*, vol. 8673. Cham, Switzerland: Springer, 2014, pp. 755–762.

[42] D. Marin, A. Aquino, M. E. Gegundez-Arias, and J. Bravo, "A new supervised method for blood vessel segmentation in retinal images by using gray-level and moment invariants-based features," *IEEE Trans. Med. Imag.*, vol. 30, no. 1, pp. 146–158, Jan. 2011.

[43] X. You, Q. Peng, Y. Yuan, Y.-M. Cheung, and J. Lei, "Segmentation of retinal blood vessels using the radial projection and semi-supervised approach," *Pattern Recognit.*, vol. 44, nos. 10–11, pp. 2314–2324, Oct./Nov. 2011.

[44] S. Aslani and H. Sarnel, "A new supervised retinal vessel segmentation method based on robust hybrid features," *Biomed. Signal Process. Control*, vol. 30, pp. 1–12, Sep. 2016.

[45] M. Schneider, S. Hirsch, B. Weber, G. Székely, and B. H. Menze, "Joint 3-D vessel segmentation and centerline extraction using oblique Hough forests with steerable filters," *Med. Image Anal.*, vol. 19, no. 1, pp. 220–249, 2015.

[46] M. Meijs *et al.*, "Robust segmentation of the full cerebral vasculature in 4D CT of suspected stroke patients," *Sci. Rep.*, vol. 7, Nov. 2017, Art. no. 15622.

[47] R. Phellan, A. Peixinho, A. Falcão, and N. D. Forkert, "Vascular segmentation in TOF MRA images of the brain using a deep convolutional neural network," in *Intravascular Imaging and Computer Assisted Stenting, and Large-Scale Annotation of Biomedical Data and Expert Label Synthesis*. Cham, Switzerland: Springer, 2017, pp. 39–46.

[48] J. Egger, Z. Mostarkic, S. Grosskopf, and B. Freisleben, "A fast vessel centerline extraction algorithm for catheter simulation," in *Proc. 20th IEEE Int. Symp. Comput.-Based Med. Syst.*, Jun. 2007, pp. 177–182.

[49] A. M. Mendonca and A. Campilho, "Segmentation of retinal blood vessels by combining the detection of centerlines and morphological reconstruction," *IEEE Trans. Med. Imag.*, vol. 25, no. 9, pp. 1200–1213, Sep. 2006.
[50] M. Lell *et al.*, "New techniques in CT angiography," *Radiographics*, vol. 26, no. 1, pp. S45–S62, 2006.
[51] K. Kamnitsas *et al.*, "Efficient multi-scale 3D CNN with fully connected CRF for accurate brain lesion segmentation," *Med. Image Anal.*, vol. 36, pp. 61–78, Feb. 2017.
[52] P. Krähenbühl and V. Koltun, "Efficient inference in fully connected CRFs with Gaussian edge potentials," in *Proc. Adv. Neural Inf. Process. Syst.*, 2011, pp. 109–117.
[53] E. Bullitt *et al.*, "Vessel tortuosity and brain tumor malignancy: A blinded study," *Academic Radiol.*, vol. 12, no. 10, pp. 1232–1240, Oct. 2005.
[54] C. Xiao, M. Staring, Y. Wang, D. P. Shamonin, and B. C. Stoel, "Multi-scale bi-Gaussian filter for adjacent curvilinear structures detection with application to vasculature images," *IEEE Trans. Image Process.*, vol. 22, no. 1, pp. 174–188, Jan. 2013.
[55] M. W. K. Law, K. Tay, A. Leung, G. J. Garvin, and S. Li, "Dilated divergence based scale-space representation for curve analysis," in *Proc. Comput. Vis. ECCV*, 2012, pp. 557–571.

**FENGJUN ZHAO** received the B.S. degree in electronic engineering and the Ph.D. degree in signal and information processing from Xidian University, Xi'an, China, in 2010 and 2015, respectively.

Since 2015, he has been a Lecturer with the School of Information Science and Technology, Northwest University, Xi'an. His research interests include medical imaging segmentation, the quantitative analysis of angiogenesis, coronary plaque detection, and the computer-aid diagnosis of breast cancer.

**YIBING CHEN** received the B.S. degree in the Internet of Things engineering from Northwest University, Xi'an, China, in 2018, where she is currently pursuing the M.S. degree in computer application technology at Northwest University.

Her current research interests include machine learning, and deep learning and their applications in medical image segmentation.

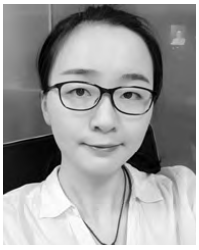

**FEI CHEN** received the B.S. degree in biomedical engineering from Xidian University, Xi'an, China, in 2015, where she is currently pursuing the Ph.D. degree in pattern recognition and intelligent system at Xidian University.

Her current research interests include convolutional neural networks, pattern recognition, and medical image processing.

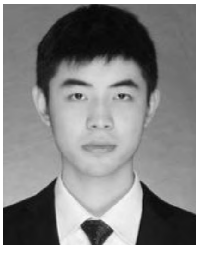

**XUELEI HE** received the B.S. degree in electronic and information engineering from Wuhan University, Wuhan, China, in 2015. He is currently pursuing the Ph.D. degree in computer application technology at Northwest University, Xi'an, China.

He has published one paper the *Journal of Biomedical Optics*. He has also applied for one Chinese invention patent. His current research interests include the development of system and algorithm in bioluminescence tomography, fluorescence molecular tomography, and X-ray luminescence tomography.

**XIN CAO** received the B.S. degree in electronic engineering and the Ph.D. degree in pattern recognition and intelligent system from Xidian University, Xi'an, China, in 2011 and 2016, respectively.

Since 2016, he has been a Lecturer with the School of Information Science and Technology, Northwest University, Xi'an. His research interests include medical image analysis and optical molecular imaging.

**YUQING HOU** received the B.S. degree from Northwest University, Xi'an, China, in 1984, and the M.S. degree from the Xi'an Institute of Optics and Precision Mechanics, CAS, Xi'an, in 1990. She is currently a Professor with the School of Information Sciences and Technology, Northwest University.

From 1993 to 2002, she was a Government-Sponsored Student with Doshisha University, Japan. From 2009 to 2010, she was a Government-Sponsored Visiting Scholar with the University of Louisville, USA. Her current research interests include digital image processing, and big data in healthcare and radiomics. She is a member of the DSP Application Expert Committee, Chinese Electronic Society.

**HUANGJIAN YI** received the B.S. degree in mathematics and applied mathematics and the Ph.D. degree in pattern recognition and intelligent system from Xidian University, Xi'an, China, in in 2008 and 2013, respectively.

Since 2014, he has been a Lecturer with the School of Information Science and Technology, Northwest University, Xi'an. His research interests include fluorescence molecular imaging and computed tomography.

**XIAOWEI HE** received the M.S. degree from the School of Electronic and Information Engineering, Xi'an Jiaotong University, Xi'an, China, in 2005, and the Ph.D. degree in pattern recognition and intelligent system from the School of Life Sciences and Technology, Xidian University, Xi'an, in 2011.

Since 2016, he has been a Professor with the School of Information Sciences and Technology, Northwest University, Xi'an. His current research interests include medical imaging processing, 3-D molecular imaging, and artificial intelligence. He is a member of the Youth Committee in Biomedical Photonics Commission, Chinese Optical Society.

**JIMIN LIANG** received the B.S. degree in electronic engineering, the M.S. degree in electronic circuit and system, and the Ph.D. degree in pattern recognition and intelligent system from Xidian University, Xi'an, China, in 1992, 1995, and 2000, respectively.

Since 2005, he has been a Professor with the School of Life Science and Technology, Xidian University. His research interests include image processing and analysis, with a focus on cardiac and auroral image analysis. Since 2013, he has been the Executive Director of the Shaanxi Society of Biomedical Engineering. He is a member of the SPIE. He has been an Editorial Board Member of the *Chinese Journal of Nuclear Medicine and Molecular Imaging* since 2011.